Time-Resolved SAXS, WAXS, and DSC Study of the Annealing of Poly(aryl ether ether ketone) (PEEK) from the Glassy State

C. Fougnies,[†] P. Damman,[†,§] D. Villers,[†] M. Dosière,[*,†] and M. H. J. Koch[‡]

Laboratoire de Physicochimie des Polymères, Université de Mons-Hainaut, Place du Parc 20, B-7000 Mons, Belgium, and European Molecular Biology Laboratory, Hamburg Outstation, EMBL c/o DESY, Notkestrasse 85, D-22603 Hamburg, Federal Republic of Germany

Received August 1, 1996; Revised Manuscript Received December 12, 1996[⊗]

ABSTRACT: The annealing of poly(aryl ether ether ketone) (PEEK) from the glassy state was investigated by time-resolved simultaneous small-angle (SAXS) and wide-angle (WAXS) X-ray scattering using synchrotron radiation and by differential scanning calorimetry (DSC). Each experiment consisted of a heating ramp from 100 °C to the annealing temperature (280, 300, 310, 315, 340, and 350 °C) at 10 °C/min, followed by a 30 min isotherm at this temperature and a cooling ramp down to 100 °C at −10 °C/min. The long spacing L and the invariant Q were estimated from the Lorentz-corrected SAXS intensity curves. The crystalline (L_c) and amorphous (L_a) thicknesses and the linear degree of crystallinity (v_c^{lin}) within the stacks of lamellar crystals were obtained from the correlation function $\gamma(r)$. The annealing temperature range can be divided into two regions based on the final morphology of the PEEK films. Samples annealed at temperatures up to 315 °C contain lamellar crystals that have crystallized during the isotherm. For annealing temperatures above 315 °C, thick lamellar crystals grow during the isotherm. However, a large fraction of the material remains molten at the end of the isotherm. The magnitude of this molten fraction increases with the annealing temperature. This molten fraction nonisothermally crystallizes during cooling as revealed by calorimetry and X-ray diffraction. The linear degree of crystallinity of PEEK crystallized from the glassy state at temperatures between 280 and 340 °C is always below 0.5, implying that the crystalline thickness of the lamellae corresponds to the smallest value of the two partial thicknesses obtained from the correlation function. For the last experiment, the polymer is fully molten at 350 °C and nonisothermally crystallizes during the cooling as revealed by calorimetry. In contrast, the analysis of the corrected invariant and the integrated WAXS intensity for this last sample indicates that the latter consists of lamellar stacks with a linear degree of crystallinity of up to 0.75.

Introduction

Poly(aryl ether ether ketone) (PEEK) is a thermoplastic with an unusual combination of high chemical resistance, excellent thermal stability, and good mechanical properties.[1−3] It can be obtained either in a fully amorphous state by quenching from the melt or in a semicrystalline state by annealing from the glassy state or by crystallization from the melt. Considerable efforts have been made to understand its crystalline structure,[4−12] morphology, and physicochemical properties[13−22] and to determine its degree of crystallinity.[23−33]

There seems to be a general agreement that semicrystalline PEEK has a dual lamellar morphology formed in two stages of crystallization, as first proposed by Bassett et al.[20] from an electron microscopic investigation of replicas of etched surfaces of PEEK films crystallized from the melt and from the glassy state. Optical microscopy observations of thin films of PEEK suggest that above 300 °C the spherulitic morphology transforms into "crystal aggregate-like structures".[21] The morphological modifications observed by electron microscopy on samples crystallized above 300 °C appear to be neither due to polymorphism nor to a modification of the lamellar growth habit, but to result from changes in lamellar thickness and stacking.[22] At crystallization temperatures below 300 °C, the spherulites consist of narrow lamellae, whereas above 300 °C, they also contain large, branched, bundle-like stretched lamellae. This change in morphology corresponds to the break near 300 °C in the graph of the density of PEEK films against the annealing temperature.[30] Melting and crystallization processes can be followed in real time by synchrotron radiation X-ray scattering, and several such studies were made on PEEK.[34−37] Hsiao et al.[35,36] reported that the low melting peak observed in the DSC scans of previously isothermally crystallized samples corresponds to a stepwise increase of the long spacing. The latter was explained by the melting of thinner lamellar crystals within the stacks of lamellae and the existence, already at the onset of the heating period, of crystals with a higher melting point.[35,36] The evolution of the X-ray scattering patterns during the isothermal crystallization of PEEK was interpreted as being due to a primary process occurring in the unrestrained melt producing thicker lamellar stacks followed by a secondary recrystallization from the restrained melt leading to thinner lamellae.[35,36]

There is, however, much controversy regarding the location of the thicker and thinner lamellae and the consecutive or competitive nature of the crystallization processes. Moreover, whereas most authors seem to favor an interpretation where the crystal thickness corresponds to the largest of the two lengths obtained from the correlation function, serious arguments have recently been presented in favor of the opposite picture.[38] Part of the confusion stems certainly from the fact that most experiments have been done using samples with different molecular weight distributions and thermal histories subjected to different rates of thermal treatment. In particular, no study of the complete crystallization cycle from the glassy state, including heating above 300 °C, isothermal annealing,

* To whom correspondence should be addressed.
† Université de Mons-Hainaut.
‡ European Molecular Biology Laboratory.
§ Research Associate of the Belgian National Fund for Scientific Research.
⊗ Abstract published in *Advance ACS Abstracts,* February 1, 1997.

S0024-9297(96)01150-3 CCC: $14.00

cooling, and melting, using identical samples is yet available. The present paper, which is devoted to the study of the thermal annealing of PEEK from the glassy state using time-resolved simultaneous small-angle (SAXS) and wide-angle (WAXS) X-ray scattering as well as differential scanning calorimetry (DSC), fills this gap. The melting of the annealed PEEK samples is described elsewhere.[39]

Experimental Section

Sheets of amorphous PEEK, with molecular weights given as $95\,000 < \bar{M}_w < 120\,000$ and $35\,000 < \bar{M}_n < 50\,000$, approximately 0.250 mm thick obtained from ICI (U.K.) were used without further treatment for the thermal annealing experiments. These amorphous samples were heated at a rate of 10 °C/min in a differential scanning calorimeter (Perkin-Elmer DSC4) and annealed at 280, 310, 315, 340, and 350 °C during 30 min.

The WAXS and SAXS curves were recorded simultaneously using two linear position detectors connected in series[40] on the X33 beam line of the EMBL in HASYLAB on the storage ring DORIS III of the Deutsches Elektronen Synchrotron (DESY) at Hamburg.[41−43] Recording times of 15 or 30 s were used to obtain the SAXS and WAXS profiles. The SAXS and WAXS intensities were recorded in the range $1/70 < s < 1/3$ nm^{-1} and $1/0.8 < s < 1/0.25$ nm^{-1}, respectively ($s = 2 \sin \theta/\lambda$, where 2θ is the scattering angle and λ the wavelength of the incident X-ray beam (0.15 nm)) using a new sample from the same batch for each thermal cycle. Calibration of the SAXS and WAXS regions were made using collagen and powders of organic compounds (benzoic acid, biphenyl, naphthalene), respectively. PEEK films wrapped in thin aluminum foils were heated in a hot stage (Mettler FP82HT) and submitted to the same thermal treatment as in the differential scanning calorimeter. The experimental X-ray intensity curves were corrected for absorption and normalized to the intensity of the primary beam monitored with an ionization chamber. A background corresponding to a fraction of the scattering of the amorphous starting sample was subtracted to remove the camera background near the beamstop. To evaluate the invariant Q and the correlation function $\gamma(r)$, the fluidlike contribution was estimated from an Is^4 versus s^4 plot and subtracted before extrapolating the SAXS intensity curves to large s values using Porod's law.[44] The integrated intensities and spacings of the (110), (111), (200), and (211) reflections were evaluated by deconvolution using the program PEAKFIT (Jandel Scientific software) after subtracting a linear background between $1.37 < s < 3.5$ nm^{-1}. The normalized intensities were Lorentz corrected by multiplying the SAXS data by s^2 and the WAXS intensities data by $\sin 2\theta \sin \theta$. The lamellar thickness L_c and the amorphous thickness L_a, the long period L, and the linear degree of crystallinity v_c^{lin} were evaluated according to standard procedures.[45,46]

Results and Discussion

Differential Scanning Calorimetry Analysis. In all experiments, the starting amorphous sample was first heated from 100 °C up to the annealing temperature (T_a), then annealed isothermally for 30 min, and, finally, cooled to 100 °C. The DSC curve of an amorphous PEEK film is shown in Figure 1. The glass transition temperature T_g and the specific heat jump at T_g (ΔC_p) are equal to 141.5 °C and 0.225 J/g·K, respectively. During heating at 10 °C/min, cold crystallization of amorphous PEEK occurs with a sharp exotherm having its extremum at 172 °C, followed by a melting−recrystallization process. Above 293 °C, the overall melting rate exceeds the overall crystallization rate. As previously shown, these characteristic temperatures (141.5, 172, and 293 °C) are strongly affected

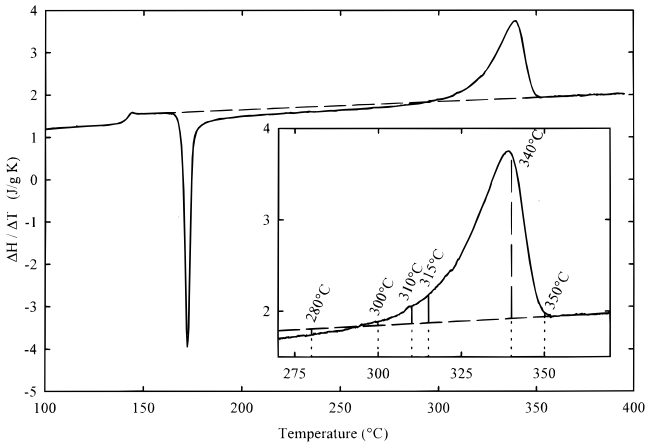

Figure 1. DSC melting curve of amorphous PEEK (heating rate: 10 °C/min). The insert is an enlargement of the melting peak, allowing estimation of the fraction of material molten upon reaching the different annealing temperatures.

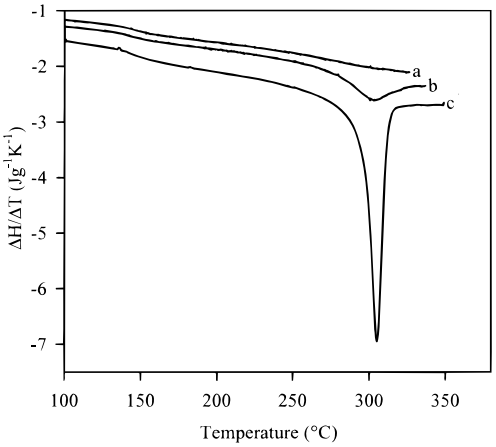

Figure 2. DSC cooling traces recorded for annealing experiments at 315 (a), 340 (b). and 350 °C (c).

by the molecular weight[16] and the heating rate but for similar experimental conditions, our values are compatible with previous reports.[16,23,47] The value of 293 °C depends somewhat on the method used to subtract the baseline. For annealing temperatures below the ones used here, a third so-called rigid amorphous phase may be present in samples crystallized between 190 and 280 °C with a maximum fraction of 14% at 190 °C. Above 280 °C, this phase no longer exists.[23] Summation of the heats of crystallization (−34.9 J/g) and melting (36.1 J/g) obtained using a straight baseline yields an estimate of about 3% for the contribution of the rigid amorphous fraction to the heat of transition. This procedure yields accurate measurements of the initial crystallinity provided the baseline passes through the liquid plateaus just above the glass transition and above the melting endotherm.[48]

Annealing temperatures above 293 °C were chosen to melt an increasing fraction of material as illustrated in the insert in Figure 1. The annealing performed at 280 °C where crystallization dominates the overall melting−crystallization process provides a reference.

The DSC cooling traces in Figure 2 indicate that for annealing temperatures of 310 °C and above, the fraction which cannot recrystallize during the isotherm crystallizes over a broad temperature range during cooling. Heats of nonisothermal crystallization of 0, −2.3, −4.9 and −24.3, and −55.5 J/g are obtained for annealings at 280, 315, 340, and 350 °C, respectively.

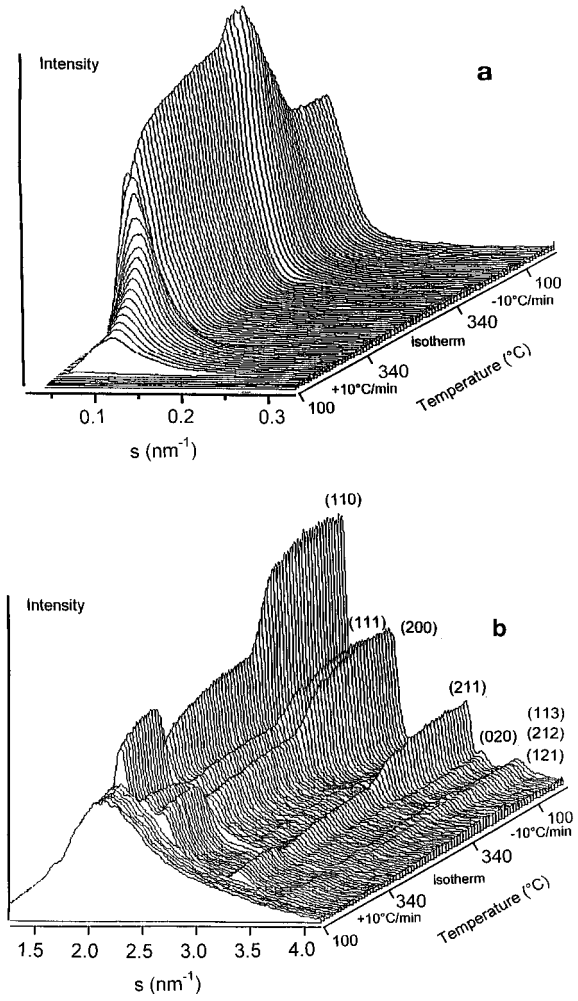

Figure 3. Untreated SAXS (a) and WAXS (b) intensity curves corresponding to the annealing of amorphous PEEK at 340 °C. The Miller indices of the WAXS reflections are indicated.

Our calorimetric results indicate that cold-crystallized PEEK samples annealed at temperatures of 315 °C and above contain two types of lamellar crystals having grown in isothermal conditions at the annealing temperature T_a and in nonisothermal conditions during cooling, respectively. These results are partially in agreement with those of Bassett et al.,[20] who observed a slight nonisothermal crystallization during cooling in their annealing experiments from the glassy state for annealing temperatures above 330 °C.

Time-Resolved X-ray Diffraction. The experimental SAXS and WAXS data recorded during annealing at 340 °C are shown in panels a and b of Figure 3, respectively.

Wide-Angle X-ray Diffraction. The peak fitting procedure used to determine the Bragg spacings and the integrated intensities from the corrected WAXS intensity curves is illustrated in Figure 4. The evolution of the unit cell parameters and the crystal density is shown in Figures 5 and 6, respectively. During heating, the *a* parameter increases from 0.795 to 0.812 nm and *b* also slightly increases from 0.592 to 0.597 nm, whereas *c* decreases from 1.020 to 0.985 nm. During the isotherm *a* may still slightly decrease whereas *b* seems to increase and *c* also decreases. During cooling, *a* and *b* decrease below their values at the onset of crystallization in the heating range, whereas *c* remains nearly constant. As a result of these changes, the crystal density is nearly constant throughout the heating range and the isotherm but rapidly increases during cooling. The lattice parameter expansion coefficients given in Table 1 were directly computed from the variation of *a*, *b*, and *c* with temperature during the cooling of the films (Figure 5). The crystalline thermal expansion coefficient α_c was also estimated from the plot of ρ_c versus temperature and is equal to 2.3×10^{-4} K^{-1}. As shown in Table 1, our values are in agreement with those previously reported by several authors.[49−52]

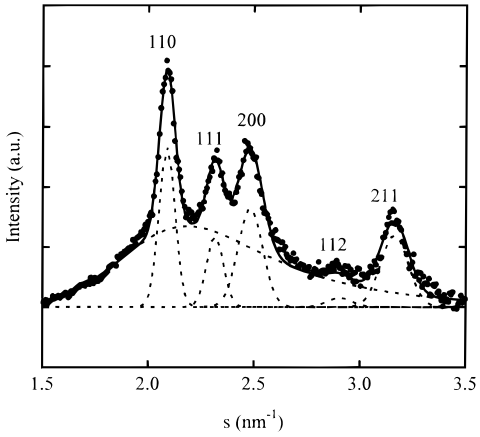

Figure 4. Illustration of the deconvolution procedure used to determine the positions and the integrated intensities of the WAXS reflections after subtraction of a linear background as indicated in the Experimental Section.

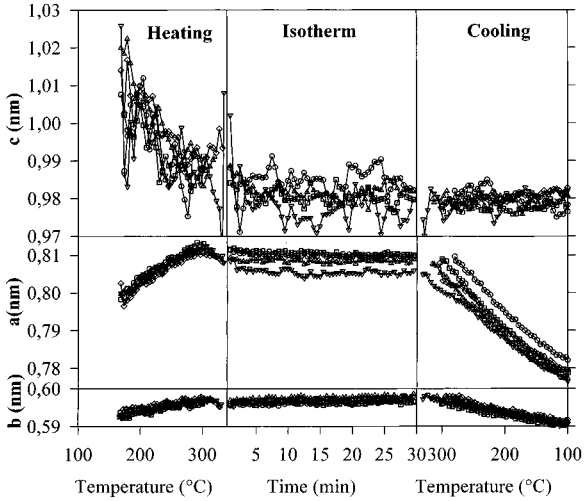

Figure 5. Variation of unit cell parameters (*a*, *b*, and *c*) of PEEK during annealing experiments at 280 (○), 300 (□), 315 (△), 340 (▽), and 350 °C (◊).

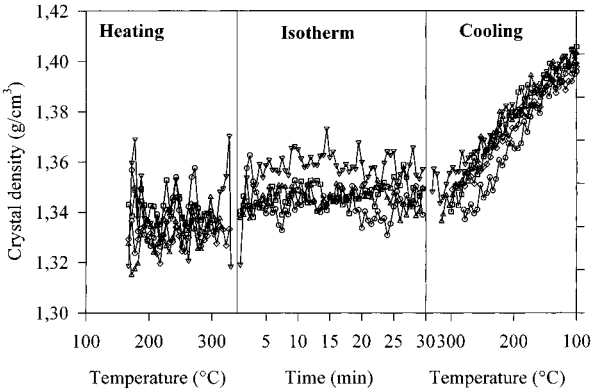

Figure 6. Evolution of crystalline density during annealing experiments at 280 (○), 300 (□), 315 (△), 340 (▽), and 350 °C (◊).

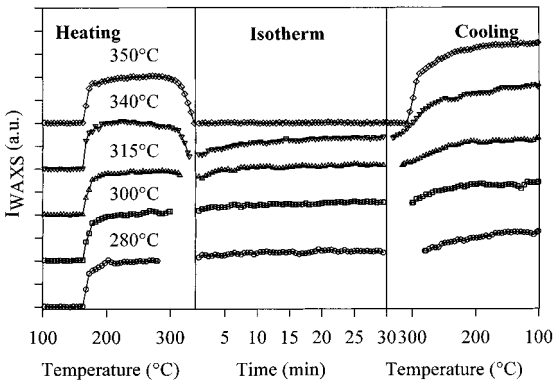

Figure 7. Evolution of the integrated WAXS intensity during annealing experiments at different temperatures as indicated. Note that the curves corresponding to different annealing temperatures have been shifted along the ordinate for better visualization.

Table 1. Thermal Expansion Coefficients of the Unit Cell Parameters *a*, *b*, and *c* (α_c^a, α_c^b, and α_c^c) and of the Crystal (α_c)

α_c^a (10^4 K^{-1})	α_c^b (10^4 K^{-1})	α_c^c (10^4 K^{-1})	α_c (10^4 K^{-1})	ref
1.33	0.39	0	1.72	51
1.56	0.66	−0.14	2.22	50
1.86	0.50	0	2.36	52
			1.80	53
1.80	0.57	0	2.37	this work

Figure 7 illustrates the evolution of the integrated WAXS intensity (I_{WAXS}). In the heating range, all curves superimpose within experimental errors as expected for identical samples treated in an identical way. There is a jump in the integrated crystalline intensity around 165 °C corresponding to the crystallization observed in the DSC curve of amorphous PEEK (Figure 1) followed by a slight increase up to 290 °C. For temperatures above 300 °C, the integrated crystalline intensity decreases and this effect is more pronounced at higher temperatures, in agreement with the progressive predominance of melting over crystallization. During the annealing isotherms, I_{WAXS} slowly increases and reaches a plateau at the end of this period. For annealing temperatures above 310 °C, the value of the integrated WAXS intensity at the end of the isotherm is always lower than the highest value recorded during the heating step. There is no crystallization during the isotherm at 350 °C as expected from DSC. The WAXS intensity analysis illustrates that only a fraction of the molten material, which depends on the annealing temperature, can crystallize during the isothermal annealing. The molten material which may be assimilated to constrained melt, partly crystallizes during the nonisothermal cooling, in agreement with the DSC analysis. This leads to an increase of the WAXS intensity during the cooling step. As already pointed out by Krüger and Zachmann[37] and illustrated in Figure 7, the integrated crystalline intensity also increases during cooling as a result of reduced thermal motion with decreasing temperature. For the sample annealed at 280 °C, where no crystallization occurs during cooling, this effect amounts to about 25% between the start and end of the cooling step. This curve provides a reference allowing estimation of the thermal disorder contribution at higher annealing temperatures. Comparison of the integrated crystalline intensity curves corresponding to cooling from 300, 315, 340, and 350 °C clearly shows that the increasingly large fraction that is still molten at the end of the isotherm, crystallizes in nonisothermal conditions during the cooling phase.

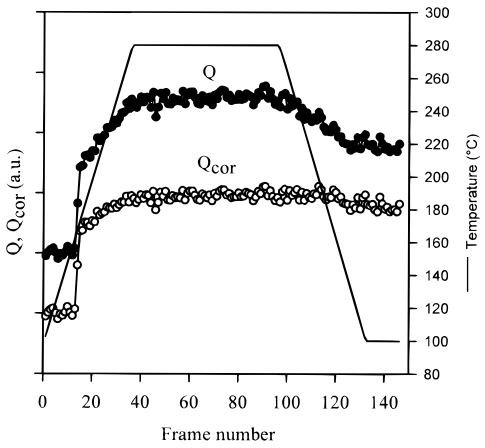

Figure 8. Variation of the uncorrected invariant (Q) and of the invariant corrected for thermal expansion (Q_{cor}) for annealing at 280 °C against frame number. The recording time was 30 s per frame.

Time-Resolved Small-Angle X-ray Diffraction. The SAXS intensity data recorded during the three phases of the annealing experiments were analyzed as follows. The invariant Q was estimated from the Lorentz-corrected SAXS intensity $I(s)s^2$ curve after subtraction of the fluidlike contribution[44]

$$Q = 4\pi \int s^2 I(s)\, ds = K v_l v_c^{lin} (1 - v_c^{lin})\, \Delta\rho^2 \qquad (1)$$

where v_c^{lin}, v_l, and $\Delta\rho$ are the linear degree of crystallinity within the lamellar stacks, the volume fraction filled with lamellar stacks, and the difference between the amorphous and crystalline densities. K is a conversion constant between electron and macroscopic densities. To take the dependence of the difference in the thermal expansion coefficients of the crystalline and amorphous regions on temperature into account, the values of Q were corrected using the relation

$$Q_{cor} = Q/[\Delta\rho(T)]^2 \qquad (2)$$

The evolution of $\Delta\rho(T)$ was estimated from a plot of $Q^{1/2}$ vs T in a temperature range where no melting occurs. The slope of this plot gives the difference between the crystalline (α_c) and amorphous (α_a) thermal expansion coefficients ($\Delta\alpha$).[53] Using the value of $\alpha_c = 2.3 \times 10^{-4}$ K^{-1} calculated from the WAXS analysis, the estimated values of the amorphous thermal expansion coefficient (α_a) below and above the glass transition T_g are 2.5×10^{-4} and 4.2×10^{-4} K^{-1}, respectively. These values are in fairly good agreement with previous reports.[38,51,52] Figure 8 illustrates the effect of the correction on the values of the invariant Q for the annealing experiment at 280 °C. The change in slope in the uncorrected cooling curve at the glass transition temperature T_g (around 145 °C) reflects the variation of the expansion coefficient of the amorphous regions above and below this temperature.

Figures 9 and 10 show the evolution of Q_{cor} and the long spacing during different annealing experiments. All curves superimpose within experimental error during their common heating range. The jump of the integrated SAXS intensity around 165 °C results from the cold crystallization of amorphous PEEK. The invariant then slightly increases up to 290 °C. Above 300 °C, melting becomes the dominant process and Q_{cor} de-

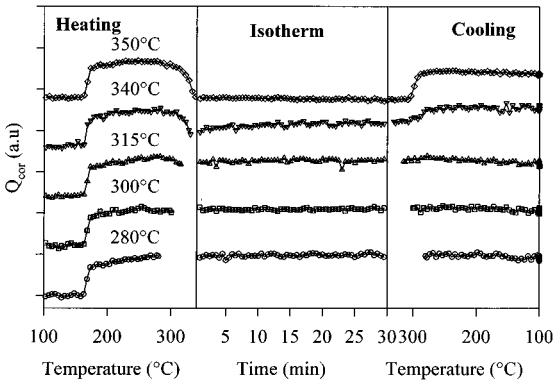

Figure 9. Evolution of the corrected invariant (Q_{cor}) during annealing experiments at different temperatures as indicated. Note that the curves corresponding to different annealing temperatures have been shifted along the ordinate for better visualization.

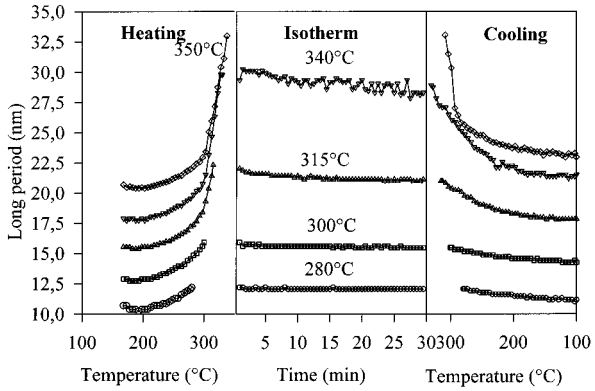

Figure 10. Evolution of the long period L determined from the maximum of the Is^2 vs s plot. For better visualization, the curves corresponding to annealing temperatures of 300, 315, 340, and 350 °C have been shifted by 2.5, 5, 7.5, and 10 nm, respectively.

creases, the effect being more pronounced at higher temperatures. During the isotherm, Q_{cor} slowly increases and finally reaches a plateau, indicating that the isothermal crystallization has stopped. The increase of the invariant Q_{cor} during the cooling step results from the nonisothermal crystallization of material that is still molten at the end of the isotherm when the annealing temperature exceeds 300 °C. This interpretation is consistent with the conclusion of the DSC and WAXS investigations given above.

To characterize the lamellar morphology of PEEK during its thermal treatment from the glassy state more completely, the correlation function $\gamma(r)$ corresponding to each SAXS intensity curve was evaluated as

$$\gamma(r) = \int I(s)s^2 \cos(2\pi sr)\, ds \qquad (3)$$

Assuming a simple two-phase model with sharp boundaries, the linear degree of crystallinity v_c^{lin} and the amorphous (L_a) and crystalline (L_c) thicknesses of the lamellae may be computed from the correlation function $\gamma(r)$ using the following relations:[45,46]

$$v_c^{lin}(1 - v_c^{lin})L = r_0 \qquad (4)$$

$$L_a = (1 - v_c^{lin})L \qquad (5)$$

$$L_c = v_c^{lin} L \qquad (6)$$

where L is the long spacing determined from the

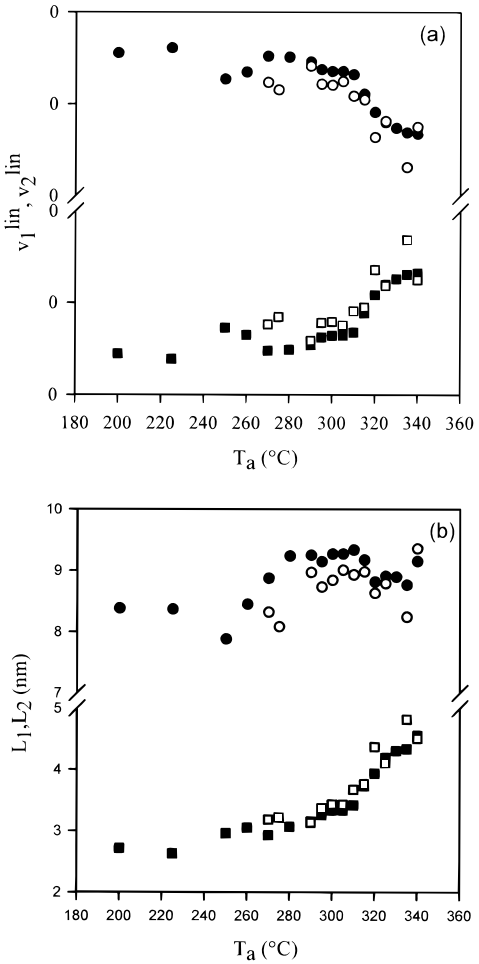

Figure 11. Dependence of the fractions v_1^{lin} (□, ■) and v_2^{lin} (○, ●) computed from the correlation function $\gamma(r)$ versus the annealing temperature T_a (a). Evolution of the corresponding thicknesses L_1 (□, ■) and L_2 (○, ●) (b). The open and filled symbols correspond to annealing time of 60 and 5 min, respectively. The SAXS intensity curves were recorded at room temperature.

position of the first subsidiary maximum of $\gamma(r)$ and r_0 the first intercept of the correlation function with the $\gamma(r) = 0$ line, respectively. Since a broad interface between the crystalline and amorphous regions very likely exists, this model may be considered as an oversimplification. Introducing additional parameters would, however, not significantly improve the accuracy of the physical parameters deduced from the correlation function.[46] Moreover, as pointed out recently by Hsiao et al.,[54] the trends in the temperature dependence of L_c and L_a remain almost unaffected. Analysis of the correlation functions does not allow one to unambiguously assign the crystalline lamellar thickness L_c to the larger or the smaller value of Lv_c^{lin} or $L(1 - v_c^{lin})$. These two hypotheses have been retained by different authors,[34,35,37,38,54] and this has, perhaps not unexpectedly, led to some controversy. A clue to the solution of this problem is provided by the analysis of the dependence of the linear crystallinity fraction v_c^{lin} on the annealing temperature. If one assumes, as one generally does for samples annealed from the glassy state, that the second melting endotherm may be assigned to the melting−reorganization process, one should also expect the lamellar thickness L_c and the crystalline fraction v_c^{lin} to increase with the annealing temperature. The evolution of v_1^{lin},v_2^{lin} and L_1,L_2 with the annealing temperature is shown in Figure 11. Since only the smallest

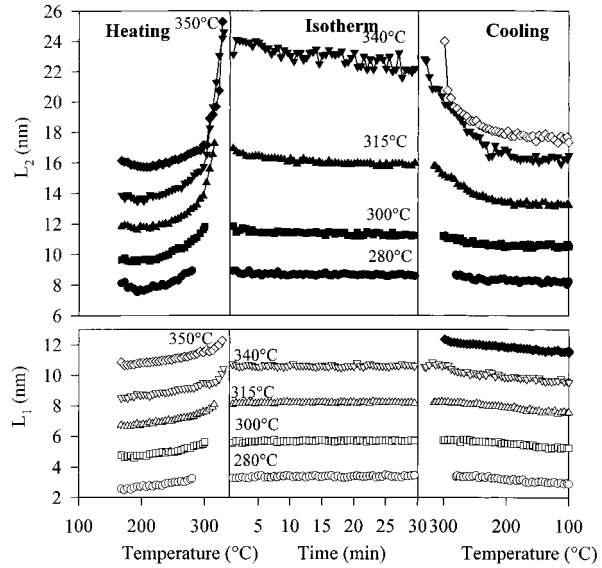

Figure 12. Evolution of the L_1 and L_2 calculated from the correlation functions during the three steps of the thermal treatment. For better visualization, the curves corresponding to annealing temperatures of 300, 315, 340, and 350 °C have been shifted by 2, 4, 6, and 8 nm, respectively. Open and filled symbols correspond to crystalline ($L_c = L_1$) and amorphous ($L_a = L_2$) thicknesses, except for the 350 °C sample.

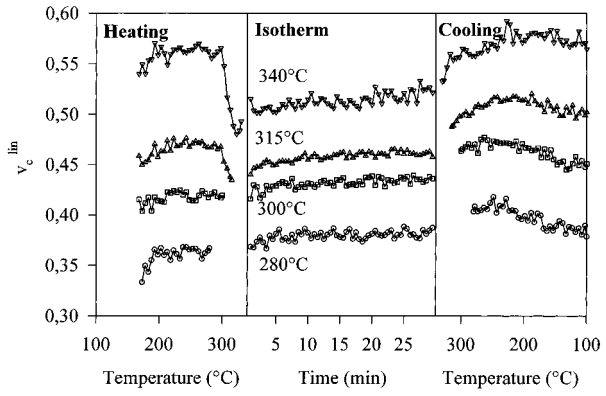

Figure 13. Variation of the linear crystalline fraction v_c^{lin} during the annealing experiments at different temperatures as indicated. The curves concerning the annealing temperatures of 300, 315, and 340 °C are shifted by 0.05, 0.10, and 0.20, respectively.

value of L_1,L_2 increases with the annealing temperature T_a, the linear degree of crystallinity must clearly be assigned to the lowest value of the thickness. Figures 12 and 13 show the evolution of $L_c = L_1$, $L_a = L_2$, and v_c^{lin} during the annealing experiments. At annealing temperatures below 350 °C, one observes that (i) during the heating step, L_c and L_a continuously increase until the annealing temperature T_a is reached whereas v_c^{lin} starts to decrease when the temperature reaches 300 °C; (ii) during the isotherm, L_c remains almost constant, v_c^{lin} increases, and L_a decreases with the annealing time; and (iii) during the cooling step, L_c and L_a decrease and v_c^{lin} increases. These observations are consistent with a model of the annealing of cold-crystallized PEEK samples where at the start of the isotherm, the initial lamellar stacks have a large amorphous thickness. As crystallization proceeds, the average distance between the crystallites L_a decreases due to the insertion of newly formed lamellae whereas the crystalline length L_c, which is determined by the annealing temperature, remains almost constant. The constraint on the melt induced by crystallization rapidly slows down the isothermal crystallization to an extent that depends on T_a and causes the plateaus in the integrated WAXS intensity (Figure 7) and the invariant Q_{cor} (Figure 9). Finally, at lower temperatures, the driving force resulting from the higher degree of supercooling increases, leading to nonisothermal crystallization.

The values of the integrated WAXS intensity I_{WAXS} and the corrected invariant Q_{cor} of the annealing at 350 °C illustrate that the material crystallized during the heating step is completely melted at such a high annealing temperature (Figures 7 and 9). Moreover, there is no crystallization up to the end of the isotherm. The increase of I_{WAXS} and Q_{cor} during the cooling is thus related to a crystallization from the melt, associated with the large exotherm in the DSC cooling curve (Figure 2). Let us note that in this last experiment the PEEK film was melted at 350 °C, which is a temperature well below the equilibrium melting temperature (around 400 °C). The heat of nonisothermal crystallization (-55.5 J·g^{-1}) for this sample is much above the maximum exotherm observed for the cold-crystallized sample (-34.9 J·g^{-1}). The bulk crystallinity of the sample, at the end of the cooling phase, is about 45% and thus much larger than the maximum crystallinity attained during heating. The value of the corrected invariant Q_{cor} at the end of the cooling step is, however, surprisingly *lower* than its maximum value during the heating step (Figure 9). The very high crystallinity of this peculiar sample, which is approximately given by the product of v_c^{lin} and the volume fraction filled with stacks v_l, implies that its linear crystallinity corresponds to the highest of both values computed from the correlation function, which is around 0.75 at the end of the cooling. The bulk crystallinity (0.45) is thus significantly smaller than the linear crystallinity in the lamellar stacks (0.75). As suggested by several authors, this observation could be related to the formation of liquid pockets associated with the stressed amorphous material constrained by the crystallization process which hinders further crystallization of the material.[54]

Conclusions

Annealing of amorphous PEEK films was investigated by simultaneous WAXS and SAXS and by DSC. The nonisothermally cold-crystallized sample has a broad single-component distribution of lamellae as indicated by the single endotherm observed in the DSC curve of an amorphous sample. The range of annealing temperatures can be divided into two regions. Below 315 °C, the lamellar crystals only crystallize during the isotherm. For annealing temperatures T_a above 315 °C, thick lamellar crystals also grow during the isotherm but a fraction of the material that increases with the annealing temperature is still molten at the end of the isotherm and crystallizes nonisothermally during the cooling phase. The linear degree of crystallinity of PEEK crystallized from the glassy state between 280 and 340 °C is always lower than 0.5. In contrast, in the case of the sample annealed at 350 °C and subsequently cooled to room temperature which effectively crystallizes from the melt in nonisothermal conditions, the analysis of Q_{cor} and I_{WAXS} unambiguously indicates that the lamellar stacks have a linear crystallinity of up to 0.75 at the end of the cooling phase.

Acknowledgment. This work was supported by the Belgian National Fund for Scientific Research and the European Union through the HCMP Access to Large Installations Project, Contract No. CHGE-CT93-0040.

References and Notes

(1) Attwood, T. E.; Dawson, P. C.; Freeman, J. L.; Hoy, L. R.; Rose, J. B.; Staniland, P. A. *Polymer* **1981**, *22*, 1096.
(2) Galli, E. *Plast. Des. Forum* **1985**, March−April, 92.
(3) Stening, T. C.; Smith, C. P.; Kimber, P. J. *J. Mod. Plast.* **1981**, 86.
(4) Dawson, P. C.; Blundell, D. J. *Polymer* **1980**, *21*, 577.
(5) Fratini, A. V.; Cross, E. M.; Whitaker, R. B.; Adams, W. W. *Polymer* **1986**, *27*, 861.
(6) Wakelyn, N. T. *Polym. Commun.* **1984**, *25*, 306.
(7) Rueda, D. R.; Ania, F.; Richardson, A.; Ward, I. M.; Balta-Calleja, F. J. *Polym. Commun.* **1983**, *24*, 258.
(8) Hay, J. N.; Kemmisch, D. J.; Langford, J. I.; Rae, A. I. M. *Polym. Commun.* **1984**, *25*, 175.
(9) Wakelyn, N. T. *J. Polym. Sci., Polym. Lett.* **1987**, *25*, 25.
(10) Hay, J. N.; Langford, J. I.; Lloyd, J. R. *Polymer* **1989**, *30*, 489.
(11) Zimmermann, H. J.; Konnecke, K. *Polymer* **1991**, *32*, 3162.
(12) Iannelli, P. *Macromolecules* **1993**, *26*, 239.
(13) Blundell, D. J.; Osborn, B. N. *Polymer* **1983**, *24*, 953.
(14) Bishop, M. T.; Karasz, F. E.; Russo, P. S.; Langley, K. M. *Macromolecules* **1985**, *18*, 86.
(15) Kumar, S.; Anderson, D. P.; Adams, W. W. *Polymer* **1986**, *27*, 329.
(16) Deslandes, Y.; Sabir, F.-N.; Roovers, J. *Polymer* **1991**, *32*, 1267.
(17) Lovinger, A. J.; Davis, D. D. *Macromolecules* **1986**, *19*, 1861.
(18) Lovinger, A. J.; Davis, D. D. *Polym. Commun.* **1985**, *26*, 322.
(19) Lovinger, A. J.; Davis, D. D. *J. Appl. Phys.* **1985**, *58*, 2843.
(20) Bassett, D. C.; Olley, R. J.; Al Raheil, I. A. M. *Polymer* **1988**, *29*, 1745.
(21) Marand, H.; Prasad, A. *Macromolecules* **1992**, *25*, 1731.
(22) Lovinger, A. J.; Hudson, S. T.; Davis, D. D. *Macromolecules* **1992**, *25*, 1752.
(23) Cheng, S. Z. D.; Cao, M.-Y.; Wunderlich, B. *Macromolecules* **1986**, *19*, 1868.
(24) Mehmet-Alkan, A. A.; Hay, J. N. *Polymer* **1992**, *33*, 3527.
(25) Voice, A. M.; Bower, D. I.; Ward, I. M. *Polymer* **1993**, *34*, 1164.
(26) Nguyen, H. X.; Ishida, H. *Polym. Compos.* **1987**, *8*, 57.
(27) Chalmers, J. M.; Gaskin, W. F.; Mackenzie, M. W. *Polym. Bull.* **1984**, *11*, 433.
(28) Cebe, P.; Chung, S.; Hong, S. D. *J. Appl. Polym. Sci.* **1987**, *33*, 487.
(29) Jonas, A.; Legras, R. *Polymer* **1991**, *32*, 2691.
(30) Damman, P.; Fougnies, C.; Moulin, J. F.; Dosière, M. *Macromolecules* **1994**, *27*, 1582.
(31) Cebe, P.; Hong, S.-D. *Polymer* **1986**, *27*, 1183.
(32) Lee, Y.; Porter, R. S.; Lin, J. S. *Macromolecules* **1989**, *22*, 1756.
(33) Blundell, D. J. *Polymer* **1987**, *28*, 2248.
(34) Wang, J.; Alvarez, M.; Zhang, W.; Wu, Z.; Li, Y.; Chu, B. *Macromolecules* **1992**, *25*, 6943.
(35) Hsiao, B. S.; Gardner, K. H.; Wu, D. Q.; Chu, B. *Polymer* **1993**, *34*, 3986.
(36) Hsiao, B. S.; Gardner, K. H.; Wu, D. Q. *Polymer* **1993**, *34*, 3996.
(37) Krüger, K.-N.; Zachmann, H. G. *Macromolecules* **1993**, *26*, 5202.
(38) Jonas, A. M.; Russell, T. P.; Yoon, D. Y. *Macromolecules* **1996**, *28*, 8491.
(39) Fougnies, C.; Damman, P.; Dosière, M.; Koch, M. H. J. *Macromolecules* **1997**, *30*, 1392.
(40) Rapp, G.; Gabriel, A.; Dosière, M.; Koch, M. H. J. *Nucl. Instrum. Methods* **1995**, *A357*, 178.
(41) Koch, M. H. J.; Bordas, J. *Nucl. Instrum. Methods* **1983**, *208*, 461.
(42) Boulin, C. F.; Kempf, R.; Koch, M. H. J.; McLaughin, S. M. *Nucl. Instrum. Methods* **1986**, *A249*, 399.
(43) Boulin, C. F.; Kempf, R.; Gabriel, A.; Koch, M. H. J. *Nucl. Instrum. Methods* **1988**, *A269*, 312.
(44) Balta-Calleja, F. J.; Vonk, C. G. In *X-ray Scattering of Synthetic Polymers*; Elsevier: Amsterdam, 1989; Chapter 7.
(45) Vonk, C. G.; Kortleve, G. *Kolloid Z. Z. Polym.* **1967**, *220*, 19.
(46) Strobl, G. R.; Schneider, M. J. *J. Polym. Sci., Polym. Phys. Ed.* **1980**, *18*, 1343.
(47) Jonas, A. Thesis, Université de Louvain-La-Neuve, Belgium, 1992.
(48) Sichina, W. J. *24th NATAS Conf., Proc.* **1995**, 375.
(49) Choy, C. L.; Leung, W. P.; Nakafuku, C. *J. Polym. Sci., Polym. Phys. Ed.* **1990**, *28*, 1965.
(50) Blundell, D. J.; D'Mello, J. *Polymer* **1991**, *32*, 304.
(51) Zoller, P.; Hehl, T.; Starkweather, H. W.; Jones, G. A. *J. Polym. Sci., Part B: Polym. Phys.* **1989**, *27*, 993.
(52) Lu, S. X.; Cebe, P.; Capel, M. *Polymer* **1996**, *37*, 2999.
(53) Fischer, E. W.; Kloos, F.; Lieser, G. *J. Polym. Sci., Polym. Lett.* **1969**, *7*, 845.
(54) Hsiao, B. S.; Sauer, B. B.; Verma, R. K.; Zachmann, H. G.; Seifert, S.; Chu, B.; Harney, P. *Macromolecules* **1996**, *28*, 6931.

MA961150Q